

Multi-user Near-Field Focusing through Time-Modulated Arrays

Rafael G. Ayestarán, Marcos R. Pino, Paolo Nepa, and Borja Imaz ^{*†‡§}

February 8, 2022

Abstract

The feasibility of a novel near-field focusing technique based on Time-Modulated Arrays (TMAs) is studied. The formulation for a near-field transmission problem is developed, showing its interesting potential for multi-user focusing at different frequencies, advantageously exploiting the characteristic TMA side frequencies radiation. Although asking for specific patterns at a set of different radiation frequencies may degrade the overall system performance, it is shown that the required radiated field distributions may still be achieved with acceptable focusing performance. This fact makes TMAs an interesting alternative to other technologies due to their simpler implementation through digital devices, also allowing for an adaptive implementation as required for many real applications. Some illustrative examples are presented.

1 Introduction

Multi-user short-range communication systems are gaining attention in recent years due to their relevance in emerging scenarios such as 5G and future 6G wireless communications, Internet of Things (IoT) and Wireless Power Transfer (WPT) [1–3], where a reliable and effective radio link between devices may be required at relatively short distances, for data and energy transmission. Among the different techniques that have been shown to allow practical implementations, Near-Field Focusing (NFF) of antenna arrays is one of the most widespread and potentially powerful [4–7]. It basically consists in concentrating radiated field power density at certain pre-assigned spots in the radiative (or Fresnel) near-field (NF) region of an antenna, so reducing the waste of energy in undesired areas/directions and limiting the far-field interference level as well. In most practical cases, and depending on different parameters such as the operating frequency, the mentioned NF region size might consist of a few centimeters or of some meters, what would allow considering scenarios such as 5G femtocells, rooms, offices, etc. where different electronic devices might be located and potentially might be wirelessly powered by a single radiating system. To do so, such radiating system, typically an antenna array or an electrically large aperture antenna, should be able to create a focal spot around the location of each device.

In order to radiate multiple devices at the same time, Near-Field Multi-Focusing (NFMF) [8–10] has been proposed as a flexible technique able to create multiple shaped focal spots at different positions of the NF region, simultaneously. It is based on the definition of a proper cost function minimized through an optimization scheme, considering as an input a mask highlighting the positions where the field must be focused, and as outputs the complex weights to be applied to the array elements. The effectiveness of the NFMF has been proved, yet a major drawback of this approach is the need for a complicated implementation of an adaptive feeding network able to change the weights of the array elements to track the moving wireless

^{*}This work was partially supported by the Spanish *Ministerio de Ciencia e Innovacion* and the Spanish Research Agency (AEI) under the projects ARTEINE (TEC2017-86619-R) and ENHANCE-5G (PID2020-114172RB-C21 / AEI / 10.13039/501100011033), and by the Gobierno del Principado de Asturias under project GRUPIN-IDI-2018-000191.

[†]This work was supported in part by the Italian Ministry of Education and Research (MIUR) in the framework of the CrossLab project (Departments of Excellence).

[‡]R. G. Ayestarán, M. R. Pino and B. Imaz are with the University of Oviedo, Department of Electrical Engineering, Gijón, Asturias, 33203 Spain (e-mail: {rayestaran,mpino}@uniovi.es).

[§]P. Nepa is with the University of Pisa, Department of Information Engineering, Pisa, 56122, Italy, and also with the Italian National Research Council (CNR), Institute of Electronics, Computer and Telecommunication Engineering (IEIIT), Turin, Italy (e-mail: paolo.nepa@uniipi.it).

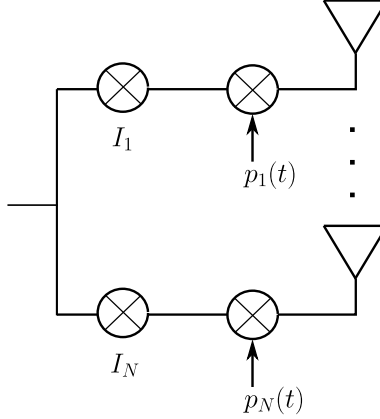


Figure 1: Time-Modulated Array: diagram of radiating elements and the applied excitations. The family of signals $p_n(t)$ represent the time-modulation at each element.

devices, especially at those relatively high frequencies requiring for expensive and high-performance amplifiers and phase shifters.

In this paper, the authors propose an alternative approach to NFMF, which allows for a much simpler hardware implementation. This approach is based on Time-Modulated Arrays (TMA) [1, 11–14], which have been proposed in recent years as an alternative to conventional arrays for digital beamforming applications, due to their simpler implementation based on digital controllers. TMAs are antenna arrays whose radiation patterns are controlled by periodically enabling and disabling the excitation of each array element instead of by applying different weights and phase shifts. The parameters associated to the control signals result not only in different effective complex weights but also in different side frequencies resulting from the pulsed modulation, each one with a proper radiated field distribution. A proper choice of the parameters defining the control signals may allow an effective control on the radiation pattern of the array at each side frequency. To the best of the authors’ knowledge, TMAs have been formulated for Far-Field (FF) problems only; moreover, some conventional formulations only account for propagation effects of the carrier frequency. Such formulations are only valid for receivers (where the side frequencies are not present in the propagated signal), which is valid for most previous works aiming at using the center frequency while minimizing the resulting side frequencies. Recently, [1], compiling and extending the work presented in [15, 16], has addressed a very exhaustive study of the transmitting properties of TMAs and their circuit implementation, taking advantage of the side frequencies to generate different beams directed towards different directions so that multiple devices may be fed through WPT at once. In this paper, we address a topic that is actually auspicated in [1] as a further application for TMAs, namely the investigation of TMAs as novel radiators to enhance the capabilities of an antenna array by adding the ability to focus the power density at precise locations in the antenna radiative NF region, at different frequencies and for multiple devices to be fed simultaneously.

2 Near-Field Transmitting Time-Modulated Arrays

The block diagram of a transmitting TMA is depicted in Fig. 1, where an array with N elements, designed with a set of static weights I_n , $n = 1 \dots N$, for a predefined function, has been considered. The most relevant parameters, plotted in Fig. 1 and Fig. 2, are as follows: the period T_0 of the pulse trains (the same period is considered for every array element); the pulse signal $p_n(t)$ used to control the n -th feeding line, acting as a switch; the normalized pulse duration $\xi_n = \tau_n/T_0$, and the normalized switch-on instant $\sigma_n = \delta_n/T_0$, where τ_n is the time-duration of the pulses in $p_n(t)$ and δ_n is their delay. Notice that the use of a pulse train may be viewed from the control point of view as a switch that enables or disables each element of the array, or from the signal processing point of view as a modulation of the carrier by using a pulse train.

TMAs, as proposed in previous works [11–14], are formulated from a far-field perspective, and they were originally intended for reception problems. Here, their use is proposed for facing NF radiation problems, by still exploiting the harmonics resulting from the transmitting signal pulse modulation. Let us consider

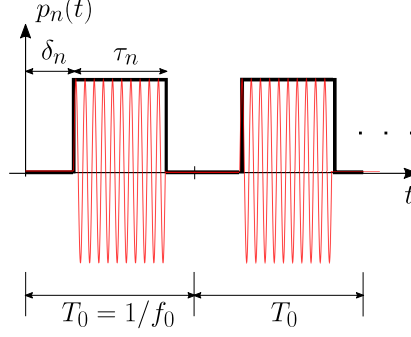


Figure 2: Time-modulated signal for the n -element of the TMA in Fig. 1, and involved parameters. The resulting RF modulated signal, $p_n(t) \cos(2\pi f_c t)$, is sketched (not in scale, as the modulation frequency is usually much smaller than the carrier frequency).

an antenna array with N elements located in the XY plane, so that the broadside direction coincides with the z -axis. The field radiated by the n -th element of an antenna array at a given frequency f_c and a given position \vec{r} in its NF region can be expressed as [17]:

$$\vec{E}_n(\vec{r}) = \vec{f}_n(\vec{r}) \frac{e^{-jk|\vec{r}-\vec{r}'_n|}}{k|\vec{r}-\vec{r}'_n|} \quad (1)$$

where $k = 2\pi/\lambda_c$ and λ_c is the wavelength corresponding to the carrier frequency f_c , i.e. $\lambda_c = c/f_c$; c is the speed of light, the position vector of the element is \vec{r}'_n , and $\vec{f}_n(\vec{r})$ for $n = 1 \dots N$ is the set of element radiated field patterns including the mutual coupling effects [18,19], in the direction defined by $\vec{r} - \vec{r}'_n$. For example, if a microstrip patch element is used, its radiation pattern can be approximated as [20]

$$\vec{f}_n(\vec{r}) = \cos \theta_n (\hat{\theta} \cos \phi_n - \hat{\phi} \sin \phi_n \cos \theta_n) \quad (2)$$

where, for a given observation point \vec{r} , the angles θ_n and ϕ_n depend on the position and orientation of the n -th radiating element located at \vec{r}'_n with respect to above observation point.

Eq. (1) can be expressed in the time domain as [17]

$$\begin{aligned} \vec{\mathcal{E}}_n(\vec{r}, t) &= \vec{f}_n(\vec{r}) \frac{\cos(\omega_c t - k|\vec{r} - \vec{r}'_n|)}{k|\vec{r} - \vec{r}'_n|} = \dots \\ &\dots = \vec{f}_n(\vec{r}) \frac{\cos[\omega_c(t - t_{dn})]}{k|\vec{r} - \vec{r}'_n|} \end{aligned} \quad (3)$$

where $t_{dn} = \frac{|\vec{r}-\vec{r}'_n|}{c}$ is the propagation delay for the n -th array element.

If a control pulse signal $p_n(t)$ is used to switch on and off the excitation applied to the radiating element, (3) becomes

$$\vec{\mathcal{E}}_n(\vec{r}, t) = \vec{f}_n(\vec{r}) p_n(t - t_{dn}) \frac{\cos[\omega_c(t - t_{dn})]}{k|\vec{r} - \vec{r}'_n|} \quad (4)$$

which is the typical pass-band signal expression whose bandwidth is defined by the frequency components of $p_n(t)$, and where it has been assumed that the antenna frequency response $f_n(\vec{r})$ is constant in the control signal frequency bandwidth. Although $p_n(t)$ bandwidth is infinite, this assumption is valid if the operational band of the TMA around ω_c is narrower than the element bandwidth, as it will be explained later in this section, and shown by the results in section 3.

Since $p_n(t)$ is a periodic signal, it can be represented by the following Fourier series:

$$p_n(t) = \sum_{q=-\infty}^{\infty} P_{nq} e^{jq\omega_0 t} \quad (5)$$

where, considering the normalized duration of the pulse and its normalized delay, P_{nq} is given by:

$$P_{nq} = \xi_n \text{sinc}(q\pi\xi_n) e^{-jq\pi(\xi_n + 2\sigma_n)} \quad (6)$$

In this expression, $\text{sinc}(x) = \sin(x)/x$, and it must be noticed that the normalized pulse duration and pulse delay must accomplish $\xi_n = \tau_n/T_0 \in (0, 1) \subset \mathbb{R}$ and $\sigma_n = \delta_n/T_0 \in [0, 1 - \xi_n] \subset \mathbb{R}$ (where \mathbb{R} is the set of real numbers). Using this representation, Eq. (3) can be expressed as

$$\vec{\mathcal{E}}_n(\vec{r}, t) = \vec{f}_n(\vec{r}) \sum_{q=-\infty}^{\infty} P_{nq} e^{jq\omega_0(t-t_{dn})} \frac{\cos[\omega_c(t-t_{dn})]}{k|\vec{r} - \vec{r}'_n|} \quad (7)$$

that can also be expressed in the frequency domain through the Fourier Transform (where $\omega = 2\pi f$ is the angular frequency) as:

$$\vec{E}_n(\vec{r}, \omega) = \pi \frac{\vec{f}_n(\vec{r})}{k|\vec{r} - \vec{r}'_n|} \dots \dots \sum_{q=-\infty}^{\infty} P_{nq} e^{-j\omega t_{dn}} \delta(\omega - q\omega_0) * [\delta(\omega - \omega_c) + \delta(\omega + \omega_c)] \quad (8)$$

and applying the convolution (*), and making use of the hermitian symmetry of P_{nq} with respect to q , it results in

$$\vec{E}_n(\vec{r}, \omega) = \pi \frac{\vec{f}_n(\vec{r})}{k|\vec{r} - \vec{r}'_n|} \dots \dots \sum_{q=-\infty}^{\infty} e^{-j\omega t_{dn}} [P_{nq} \delta(\omega - \omega_c - q\omega_0) + P_{nq}^* \delta(\omega + \omega_c + q\omega_0)] \quad (9)$$

where $(.)^*$ denotes the complex conjugate operator. It can be observed how the side frequencies $\pm q\omega_0$ resulting from (5) are present through the resulting *delta* functions. Accounting only for the positive frequencies in (9) leads to

$$\vec{E}_n(\vec{r}, \omega_+) = \pi \frac{\vec{f}_n(\vec{r})}{k|\vec{r} - \vec{r}'_n|} \dots \dots \sum_{q=-\infty}^{\infty} P_{nq} e^{-j(\omega_c + q\omega_0)t_{dn}} \delta(\omega - \omega_c - q\omega_0) \quad (10)$$

where the harmonics or side-frequencies can be explicitly observed together with the carrier frequency. The use of switches results in side frequencies due to the Fourier series-representation of the rectangular pulses, and hence in different frequencies that might be used to generate different radiation patterns. In most previous works [11–14], TMAs are used as receivers or make use of the receiving formulation. In such cases, only the carrier frequency ($q = 0$) is transmitted, and hence there are no side frequencies in the spectrum of the propagating wave signal. According to the formulation, the received signal consists of a single frequency, f_c , while side frequencies are the result of the processing held inside the receiver through the pulse modulation. On the other hand, when considering a transmitting TMAs, the side frequencies are present in the radiated signal, and this fact has to be accounted for when formulating the propagation model, as apparent in eq. (10).

It is worth noticing that the observation point \vec{r} has been assumed in the far-field region of each array element, yet not so far from the array so that it is in the array Fresnel region [7]. This assumption allows considering the FF radiation pattern for the array elements to evaluate its contribution in the array NF region.

From expression (10), phasor notation may be used to express the total field radiated by the array at one of the frequencies defined by q (i.e., $\omega_c + q\omega_0$) using

$$\begin{aligned}
\vec{E}(\vec{r}, \omega_c + q\omega_0) &= \sum_{n=1}^N I_n \vec{E}_n(\vec{r}, \omega_c + q\omega_0) \\
&= \sum_{n=1}^N I_n \vec{f}_n(\vec{r}) P_{nq} \frac{e^{-j(\omega_c + q\omega_0)t_{dn}}}{k|\vec{r} - \vec{r}'_n|} \\
&= \sum_{n=1}^N I_n \vec{f}_n(\vec{r}) F_n(\vec{r}, \omega_c + q\omega_0)
\end{aligned} \tag{11}$$

where I_n are the static weights corresponding to each element of the array, and

$$\begin{aligned}
F_n(\vec{r}, \omega_c + q\omega_0) &= \xi_n \text{sinc}(q\pi\xi_n) \dots \\
&\dots e^{-jq\pi(\xi_n + 2\sigma_n)} \frac{e^{-j(\omega_c + q\omega_0)t_{dn}}}{k|\vec{r} - \vec{r}'_n|}
\end{aligned} \tag{12}$$

Equation (11) can be used to synthesize the required NF distributions, as it depends on all the parameters that may be tuned in the system. From (12), the component under study of the field expressed in the time-domain is

$$\vec{E}_n(\vec{r}, t) = \vec{f}_n(\vec{r}) \sum_{q=-\infty}^{\infty} F_n(\vec{r}, \omega_c + q\omega_0) e^{jq\omega_0 t} \tag{13}$$

which represents the n -th element E -field complex envelope respect to f_c . Then, the total E -field complex envelope respect to f_c is straightforward:

$$\vec{E}(\vec{r}, t) = \sum_{n=1}^N I_n \vec{E}_n(\vec{r}, t) \tag{14}$$

and the radiated field is

$$\vec{\mathcal{E}}(\vec{r}, t) = \Re \left\{ \vec{E}(\vec{r}, t) e^{j\omega_c t} \right\} \tag{15}$$

According to (11) and (12), the resulting effective weights $P_{nq} \in \mathbb{C}$, or their parameters $\xi_n, \sigma_n \in \mathbb{R}$ may be calculated to achieve different behaviors at each frequency $f_c + qf_0$. Through a proper synthesis scheme, the system parameters might be calculated so that different specifications are fulfilled for the different frequencies. However, equation (6) shows that in the case of the carrier frequency ($q = 0$) the phase of the resulting effective weights is inevitably null, so very limited control over its radiation pattern can be achieved. Time-modulation may be considered as an enhanced capability added to an array already designed according to some requirements for the carrier, for example for information transfer, fulfilled by using the static weights I_n ; the resulting side frequencies may then be exploited for additional wireless power transfer to other devices of the scenario.

Some simulations have been carried out to verify if the suitable control over the pulse signals and the corresponding effective array weights is enough to allow a certain degree of control on the resulting side-frequency patterns. If so, TMAs might be used to implement adaptive systems, modifying the pulse parameters through a digital controller, and so avoiding expensive high frequency devices, such as variable attenuators, amplifiers and phase shifters.

In the procedure shown in equations (1) to (13), the array elements are modeled by a radiation pattern constant with frequency (2). This approach can be considered valid in a practical case if a limited set of side-frequencies are used (the array element bandwidth covers all this set of side-frequencies). For this reason, a limited set of values of q (i.e. a limited set of side-frequencies) will be used ensuring the validity of this assumption. It is noteworthy that the side-frequencies are ruled by a *sinc* function resulting from eq. (6). This fact leads to a decreasing amplitude with $|q|$. It can be compensated by the synthesis method by finding a set of effective weights P_{nq} whose resulting power is compensated across the range of frequencies

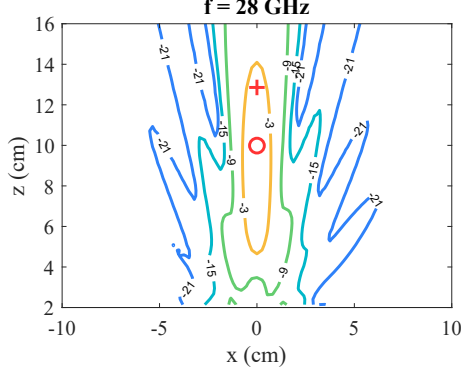


Figure 3: Normalized Near Field distribution at $y = 0$ with a focal point at $(x, y, z) = (0, 0, 12)\lambda_c$ at the carrier frequency designed using the a conventional NFF method in an 8×8 patch-element array without time-modulation. The symbols $+$ and \circ represent the assigned focal point and the synthesized field maximum point, respectively. The contour of the -3dB spot is denoted by the brown line.

(i.e. the range of values of q) provided that it is relatively short, but if a too high number of side-frequencies are used the compensation might not be feasible. This fact represents a more limiting reason for using a range of frequencies than the assumption of a constant $f_n(\vec{r})$, as the latter can account for the frequency response of the array elements with no additional cost.

If the antenna response cannot be considered constant along the frequency range of the set of side-frequencies, the radiation pattern of the antenna will be frequency dependent modeled by $f_n(\vec{r}, \omega)$. In this case, the eqs. (1), and (7) to (9) showing the fields in frequency domain should be modified by substituting $f_n(\vec{r})$ by an expression accounting for the frequency variation $f_n(\vec{r}, \omega)$ so that each harmonic $w_c \pm q\omega_0$ is affected by the corresponding antenna response. In time domain expressions, the antenna element time response should be included. The use of frequency-dependent models will be subject of a future study.

3 Simulation results

Some simulations have been carried out to evaluate the suitability of TMAs for multi-user focusing. In all cases, an antenna array with 8×8 microstrip patch elements is considered, with radiation properties approximated by (2), and with interelement distance $d = 0.7\lambda_c$, where $\lambda_c = c/f_c$ is the free-space wavelength at the carrier frequency of 28GHz. The fundamental frequency for the pulse signal is set at 200MHz ($T_0 = 5$ ns). The antenna has been designed to focus at $(x, y, z) = (0, 0, 12)\lambda_c$ for information transfer at the carrier frequency, so the set of required static weights I_n has been obtained using a conventional NFF method [6]. Its corresponding NF distribution is represented in Fig. 3.

The pulse signals required for each set of specifications can be determined by solving a proper optimization problem, and many different approaches can be used. Since we are interested just to verify the focusing capabilities of the TMAs, a simple brute-force direct optimization has been here applied to the following minimization problem:

$$\underset{\xi_n, \sigma_n}{\text{minimize}} \left\{ \left\| \left| \tilde{\mathbf{E}} \right| - \mathbf{E}_{target} \right\|^2 \right\} \quad (16)$$

subject to

$$\begin{aligned} \xi_n &\in (0, 1) \subset \mathbb{R} \\ \sigma_n &\in [0, 1 - \xi_n] \subset \mathbb{R} \end{aligned}$$

where $\tilde{\mathbf{E}} = [\dots; \mathbf{E}_q; \dots]$ is a stacked version of the matrices \mathbf{E}_q containing the samples of the field level $|E(\vec{r}, \omega_c + q\omega_0)|$ for each considered frequency in the NF region (including the carrier to ensure that its behavior is not significantly modified by the time-modulation), and \mathbf{E}_{target} is a matrix with the same size containing zero values except for the samples corresponding to the assigned focal points, where a unitary

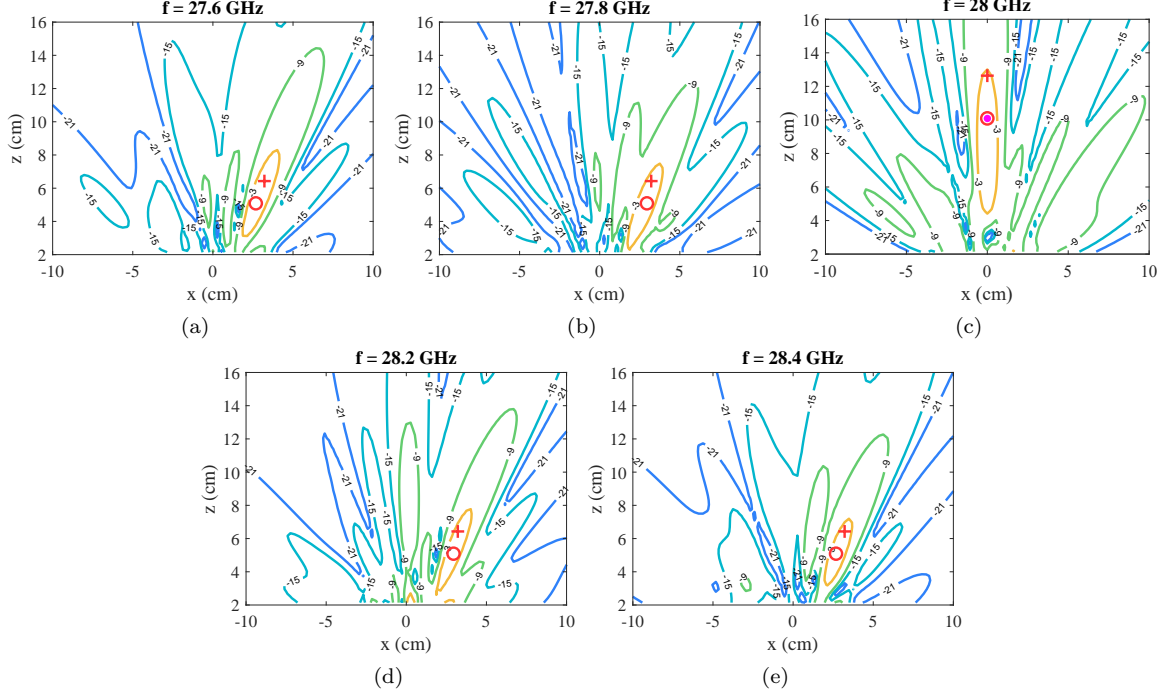


Figure 4: Simulation #1. Normalized Near Field distribution at $y = 0$ with a focal point at $(x, y, z) = (3, 0, 6)\lambda_c$ at all the considered frequencies. The field level at each frequency is normalized with respect to the overall maximum level. The symbols $+$ and \circ represent the assigned focal point and the synthesized field maximum point, respectively. The overall maximum used as reference for the field level is represented with a filled magenta circle. The contour of the -3dB spot is denoted by the brown line.

value is set to enforce a higher field level. This minimization outputs the parameters ξ_n and σ_n required in the pulse signals to generate a near field distribution with amplitude as similar as possible to \mathbf{E}_{target} with the given array. Using the amplitude of the obtained field distribution allows considering such unitary value, but it is also necessary because otherwise an equal null phase would be enforced at the focal points. Neither an equal phase nor a null phase is necessary, so using the amplitude of the field avoids an unnecessary constraint. The region considered for the optimization has been limited to $x, y \in [-10\lambda_c, 10\lambda_c], z \in [0, 15\lambda_c]$ sampled each $0.2\lambda_c$. This is a very simple and non-refined optimization based on [9, 21], used just for testing purposes.

3.1 Simulation #1. Equal focus at all side frequencies.

In simulation #1, the same single focal point has been assigned at $(x, y, z) = (3, 0, 6)\lambda_c$ for a set of four frequencies ranging from 27.6GHz to 28.4GHz, with a 200MHz separation, and excluding the carrier (28GHz). This simulation is intended as a first test for the focusing capabilities of the TMA, but it might also correspond to a case where a single user located at the focal point must be fed. The focal points have been assigned in the plane $y = 0$ to facilitate the representation of the resulting radiated field distributions.

The optimization (16) results in the NF distributions are plotted in Fig. 4 for $y = 0$, where the field level at each frequency is normalized to the overall maximum radiated level. It may be noticed that both the specified focal points and the obtained maximum points are located within the -3dB spot. The carrier frequency is also represented to verify that it keeps focused at the assigned focal point $(0, 0, 12)\lambda_c$.

The focusing performance is evaluated through two standard figures of merit, the depth of focus (DoF) and the width of focus (WoF) [22], i.e. the length and width of the resulting -3dB focal spots. The results are summarized in Table 1, where the field level at the focal points normalized with respect to the overall maximum and to the maximum achieved in the same focal spot, at the same frequency, are also indicated. Additionally, the transverse field distribution across the radial line passing through the focal

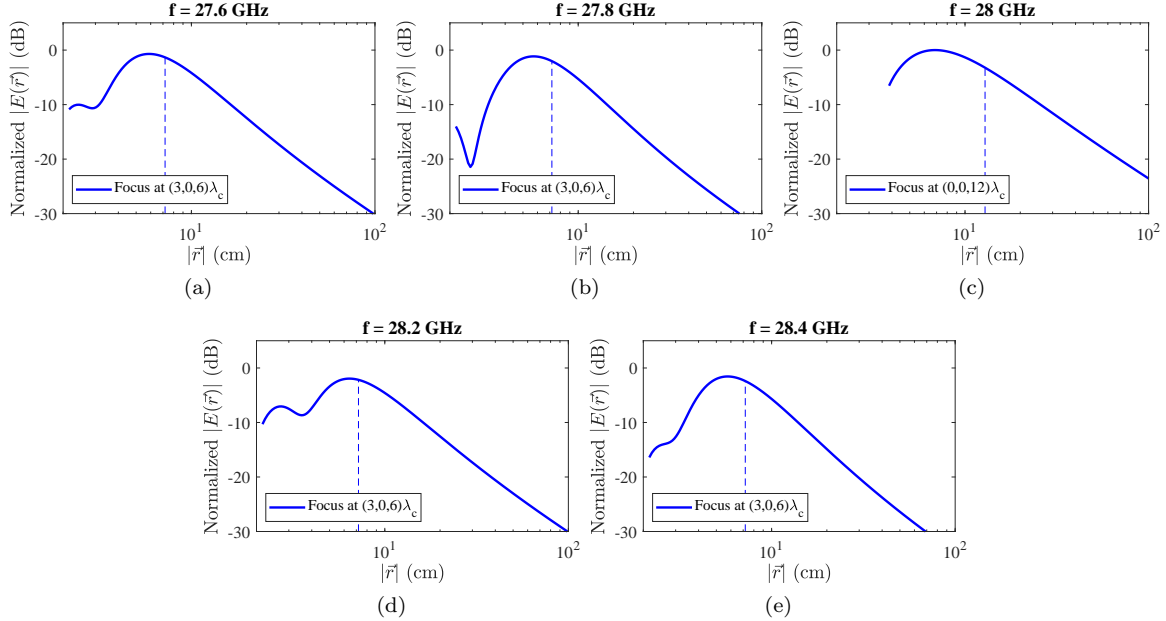


Figure 5: Simulation #1. Normalized Near Field distribution radiated by the TMA across the axis from the origin through the focal point, at all five frequencies. The position of the assigned focal point $(x, y, z) = (3, 0, 6)\lambda_c$ is shown by the dashed line.

points is represented in Fig. 5.

Freq	$ \tilde{E} _{dB}$	$ \tilde{E}_r _{dB}$	DoF _t	WoF _t	DoF _w	WoF _w
27.6 GHz	-1.0	-0.9	5.4	1.0	3.7	1.3
27.8 GHz	-1.7	-1.5	5.4	1.0	3.7	1.2
28.2 GHz	-1.8	-1.0	5.1	0.8	3.7	1.2
28.4 GHz	-2.0	-1.1	4.0	0.9	3.7	1.2

Table 1: Simulation #1. Depth and width of focus, in cm, when the same focus at $(x, y, z) = (3, 0, 6)\lambda_c$ has been assigned at a set of four frequencies ranging from 27.6GHz to 28.4GHz, except for the carrier. The subscript t refers to a TMA radiating as shown in Fig. 4, while the subscript w refers to a conventional weigh-based array radiating as shown in Fig. 6. The field amplitude at the focus normalized with respect to the overall maximum (located at 28GHz), $|\tilde{E}|$, and relative to the peak value at the focal spot at the same frequency, $|\tilde{E}_r|$, are also expressed (in dB).

The more demanding requirements with respect to a conventional single-frequency focusing problem might affect the performance of the TMA, so a comparison has been carried out. It is important to notice that conventional NF focusing is intended for only one frequency, so four independent simulations have been considered, one for each side-frequency, leading to four independent sets of weights. This fact implies that a fair comparison of performance is not possible, although it allows an initial guess of the accuracy of TMAs in focusing. Fig. 6 shows the four independent field distributions obtained using the same brute force optimization algorithm (16) for each frequency. The resulting DoF and WoF are presented in Table 1. As it is expected, the four independent optimizations get similar results, and the resulting spots are only slightly smaller than those obtained with a TMA. However, the performance loss using TMAs, which are required to concurrently match the focusing requirements at four different frequencies, only results in a slight increase of the DoF.

It is noteworthy that the original behavior at the carrier frequency has also been modified. Using the side frequencies leads to a power sharing between all the frequencies instead of just radiating at a single

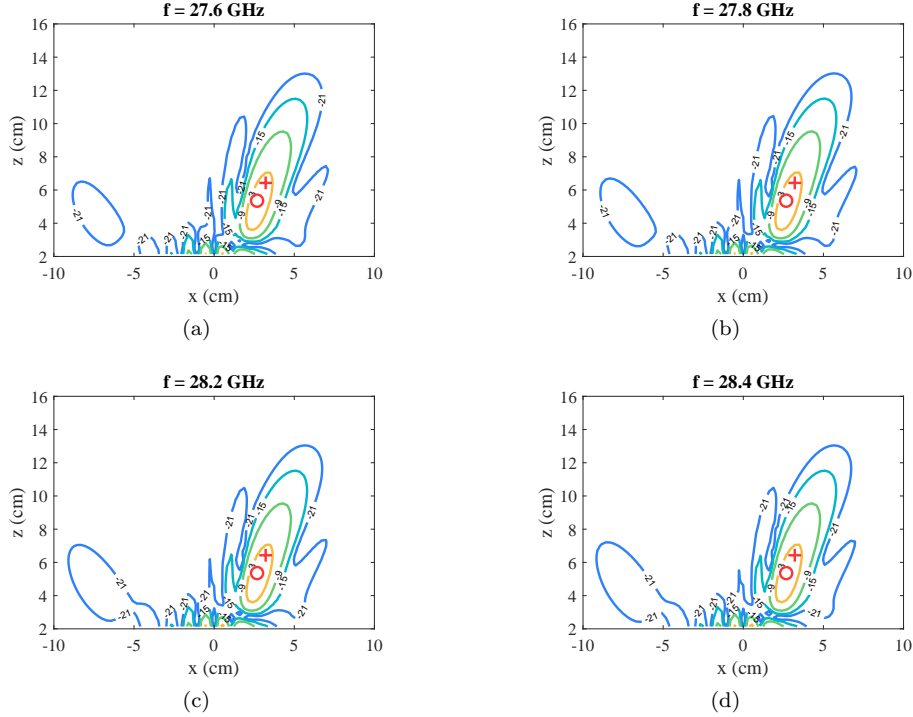


Figure 6: Simulation #1. Normalized Near Field distribution at $y = 0$ obtained with four conventional NF focused arrays, each one synthesized independently to focus at $(x, y, z) = (3, 0, 6)\lambda_c$. The field level at each frequency is normalized with respect to the overall maximum level. The symbols $+$ and \circ represent the assigned focal point and the synthesized field maximum point, respectively. The contour of the -3dB spot is denoted by the brown line.

frequency. It results in a reduced spot, with smaller DoF and WoF, as summarized in Table 2. However, focusing is still achieved at the desired location, and even a reduction of the waste of energy at undesired locations is achieved as a collateral effect.

A full-wave simulation has been carried out to evaluate the accuracy of the model in simulation #1 in more realistic conditions and accounting for coupling effects, accurate element patterns, etc. A coaxial-fed microstrip patch working at a center frequency of 28GHz has been designed using CST Studio Suite. The substrate material is Rogers DT/Duroid 5880, with a dielectric constant of 2.2 and a loss tangent of 0.00009. With this patch model, an 8×8 element array has been generated according to the above structure. The array model has been simulated at every assigned q -harmonic ($q = 0$ for the carrier) when the feeding current distribution is proportional to the effective weights $I_n \cdot P_{nq}$ obtained after solving the optimization problem in (16). The synthesized pulse parameters are used to obtain the values P_{nq} through eq. (6). The resulting field distributions are presented in Fig. 7, where it can be noticed that the proposed model (2) extracted from [20], though quite simple, is enough accurate for testing TMA capabilities. Obviously, the

Freq	DoF _t	WoF _t	DoF ₀	WoF ₀
28 GHz	8.5	1.2	9.3	1.5

Table 2: Simulation #1. Depth and width of focus, in cm, for the focus at $(x, y, z) = (0, 0, 12)\lambda_c$ assigned at the carrier frequency 28GHz. The subscript t refers to a TMA radiating as shown in Fig. 4, while the subscript 0 refers to a conventional weight-based array synthesized only for the carrier frequency as shown in Fig. 3.

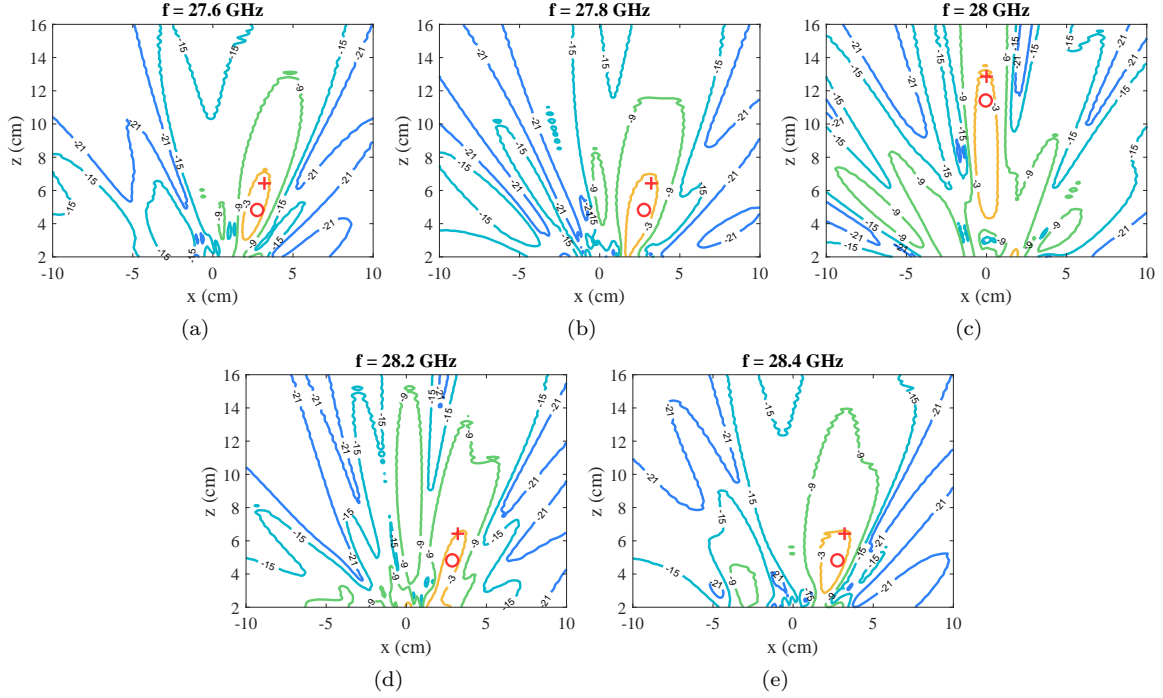


Figure 7: Full-Wave Simulation #1. Normalized Near Field distribution at $y = 0$ with a focal point at $(x, y, z) = (3, 0, 6)\lambda_c$ at all the considered frequencies. The field level at each frequency is normalized with respect to the overall maximum level. The symbols $+$ and \circ represent the assigned focal point and the synthesized field maximum point, respectively. The contour of the -3dB spot is denoted by the brown line.

more accurate is the model $\vec{f}_n(\vec{r})$ (or $\vec{f}_n(\vec{r}, \omega)$) of the array, the more accurate will be the results without any change in the specific TMA formulation.

3.2 Simulation #2. Four-spot case.

In simulation #2, a multi-user problem is considered. Four different focal points have been assigned, each one at a different frequency in the above range 27.6-28.4GHz. Assigned focal points are represented in Table 3, where all the distances are referred to the wavelength at the carrier frequency. The 8×8 element-array, and the operating and fundamental frequencies are the same as for simulation #1. The resulting field distributions are represented in Fig. 8.

q	Freq	Focal point	Focal point (cm)
-2	27.6 GHz	$(-3, 0, 9)\lambda_c$	$(-3.21, 0, 9.64)$
-1	27.8 GHz	$(4, 0, 7)\lambda_c$	$(4.29, 0, 7.50)$
1	28.2 GHz	$(0, 0, 10)\lambda_c$	$(0, 0, 10.71)$
2	28.4 GHz	$(-4, 0, 7)\lambda_c$	$(-4.29, 0, 7.50)$

Table 3: Simulation #2. Frequency distribution for the focal points in the case with four users.

The pulse parameters are obtained through optimization resulting in the NF distributions plotted in Fig. 8 for $y = 0$. Again, it may be observed that all the focal points and synthesized maximum points lay within the -3dB spot. The field distribution across the axis passing through the focal points is plotted in Fig. 9, while the resulting figures of merit are summarized in Table 4.

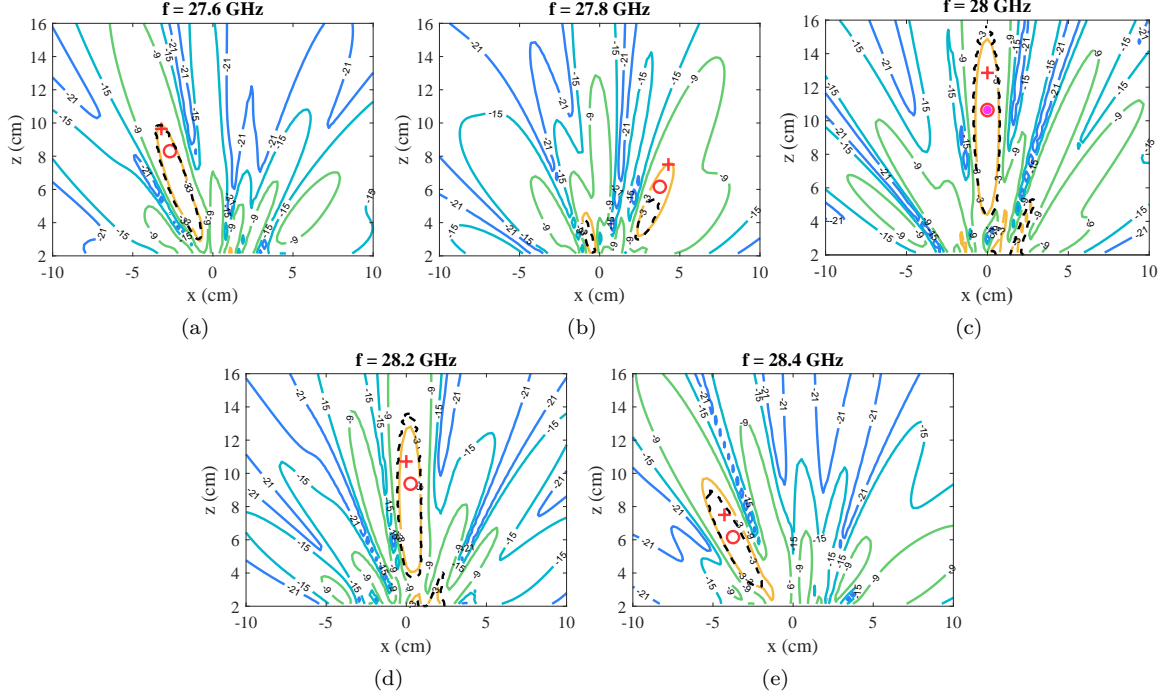


Figure 8: Simulation #2. Normalized Near Field distribution at $y = 0$ in the case with four users. The field level at each frequency is normalized with respect to the overall maximum level. The symbols $+$ and \circ represent the assigned focal point and the synthesized maximum point, respectively. The overall maximum used as reference for the field level is represented with a filled magenta circle. The contour of the -3dB spot is denoted by the brown line. The -3dB spot obtained through full-wave simulations is denoted by the black dashed line.

3.3 Simulation #3. Five-spot case with two spots at one side frequency.

A further case, simulation (#3), involving five users is performed. Four frequencies are assigned, each corresponding to a user except for one of them, corresponding to $q = -1$, where two users, namely two different focal spots, are assigned. Although a typical application would require a single user per frequency assignment, this example is intended to test multi-focusing capabilities at a given frequency. The focal points have also been specified according to the frequency distribution shown in Table 5. Although the number of requirements is notably increased, the results in Fig. 10 show that the TMA is still able to provide a field distribution with maxima laying into -3dB spots and with a small focal shift. The resulting figures of merit are summarized in Table 6.

Freq	Focal point	DoF	WoF	$ \tilde{E} _{dB}$	$ \tilde{E}_r _{dB}$
27.6 GHz	$(-3, 0, 9)\lambda_c$	7.3	1.1	-2.7	-1.1
27.8 GHz	$(4, 0, 7)\lambda_c$	4.7	1.1	-2.9	-1.3
28.2 GHz	$(0, 0, 10)\lambda_c$	8.5	1.3	-1.6	-1.0
28.4 GHz	$(-4, 0, 7)\lambda_c$	7.8	1.3	-0.6	-0.6

Table 4: Simulation #2. Depth and width of focus, in cm, for the case with four users at four frequencies. The field amplitude at the focus normalized with respect to the overall maximum (located at the carrier), $|\tilde{E}|$, and relative to the peak value in the focal spot at the same frequency, $|\tilde{E}_r|$, are also expressed (in dB).

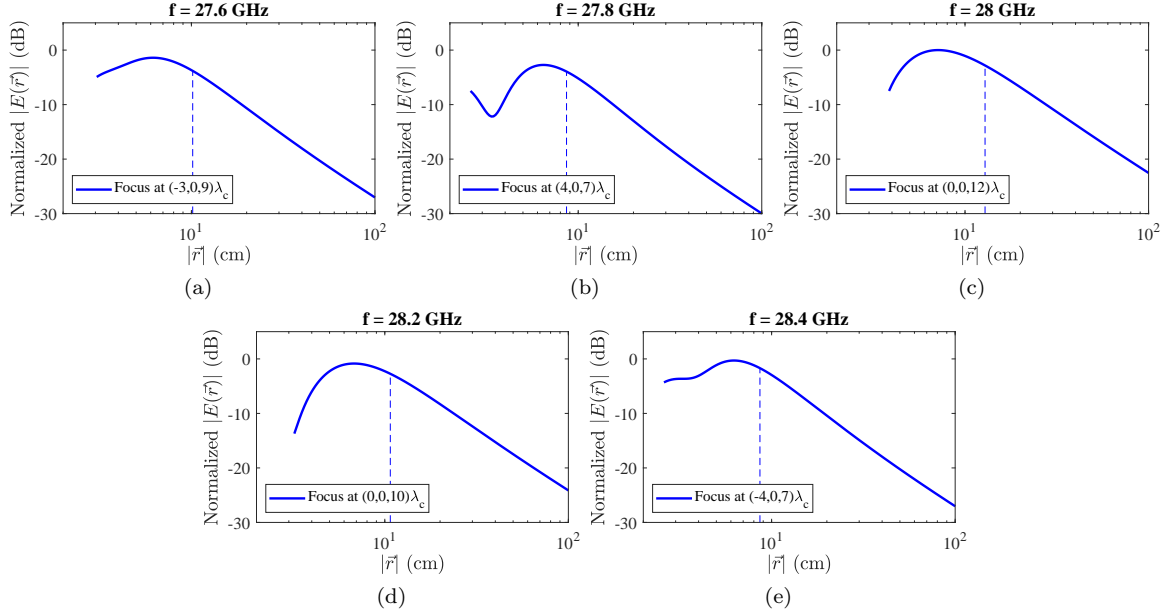


Figure 9: Simulation #2. Normalized Near Field distribution across the axis from the origin through the focal points, at all four assigned frequencies. The position of the focal points (see Table 3) is denoted by a dashed line.

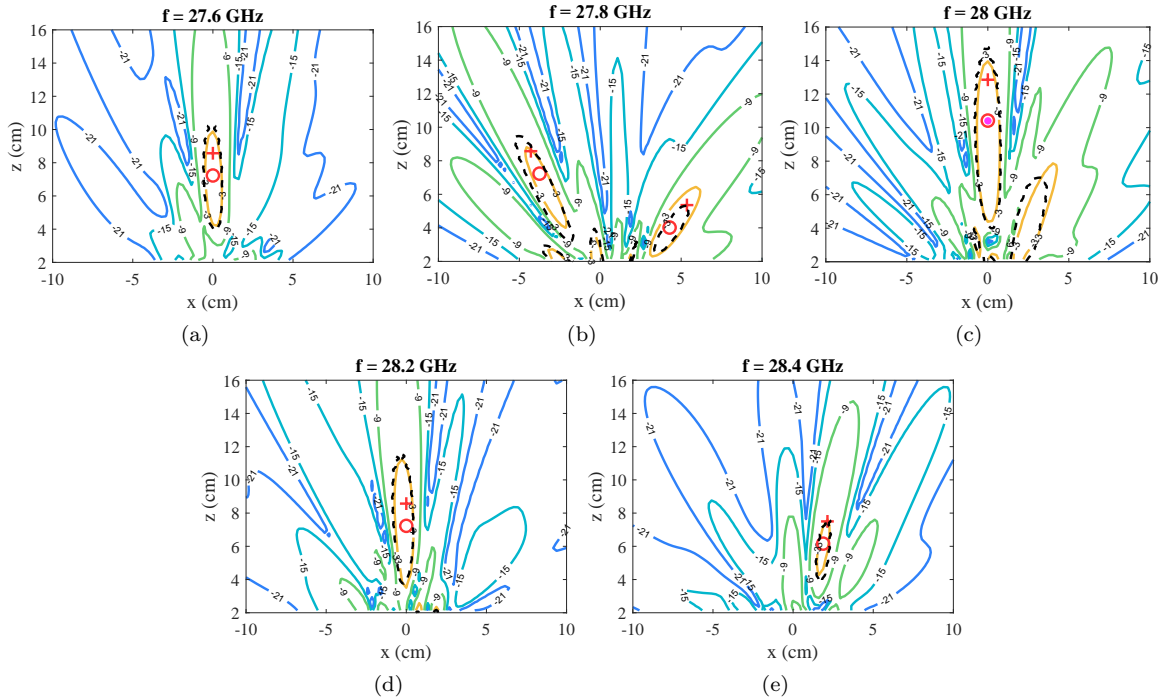


Figure 10: Simulation #3. Normalized Near Field distribution at $y = 0$ in the case with five users, two of them assigned for 27.8GHz. The field level at each frequency is normalized with respect to the overall maximum level. The symbols $+$ and \circ represent the assigned focal point and the synthesized field maximum point, respectively. The contour of the -3dB spot is denoted by the brown line. The -3dB spot obtained through full-wave simulations is denoted by the black dashed line.

q	Freq	Focal point	Focal point (cm)
-2	27.6 GHz	$(0, 0, 8)\lambda_c$	$(0, 0, 8.57)$
-1	27.8 GHz	$(-4, 0, 8)\lambda_c$	$(-4.29, 0, 8.57)$
		$(5, 0, 5)\lambda_c$	$(5.36, 0, 5.36)$
1	28.2 GHz	$(0, 0, 8)\lambda_c$	$(0, 0, 8.57)$
2	28.4 GHz	$(2, 0, 7)\lambda_c$	$(2.14, 0, 7.50)$

Table 5: Simulation #3. Frequency distribution for each focal point in the case with five users, two of them assigned for 27.8GHz.

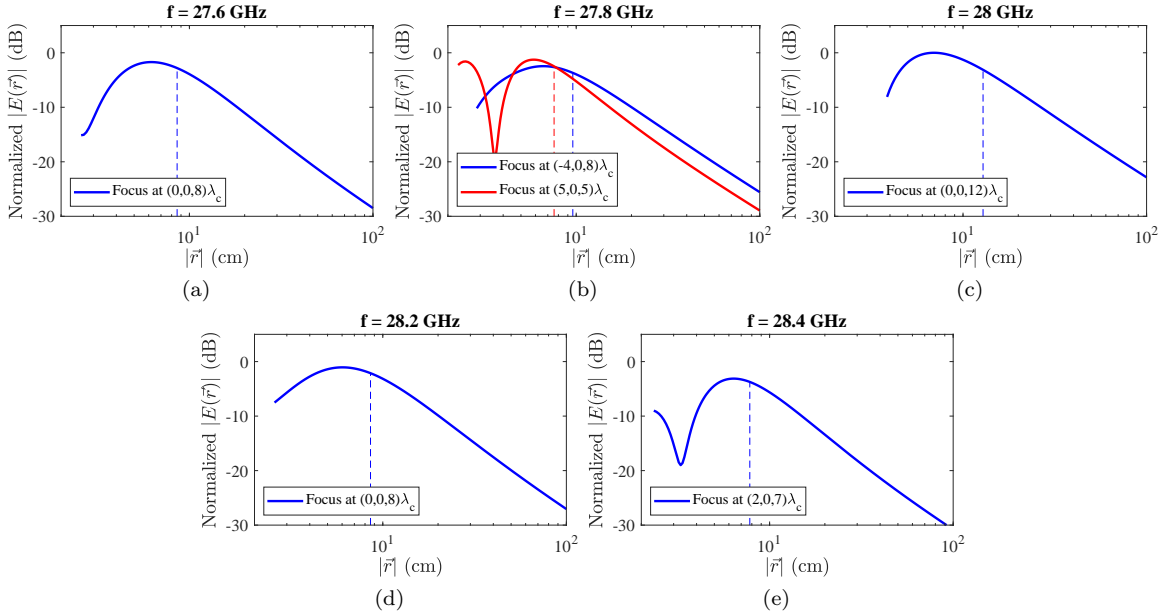


Figure 11: Simulation #3. Normalized Near Field distribution across the axis from the origin through the focal points, at all four frequencies in the case with five users. Two distributions may be observed for 27.8GHz. The position of the focal points is denoted by the dashed line.

3.4 Simulation #4. Equal focus at all frequencies

The previous simulations have been modified to check the effect of using a different set of values I_n (i.e. the static weights of the array before applying time-modulation). These values have been calculated using the optimization method in [8] to get two spots at the carrier frequency located at $(x, y, z) = (0, 0, 12)\lambda_c$ and $(x, y, z) = (3, 0, 6)\lambda_c$ simultaneously. For the four side frequencies, a focal point at $(x, y, z) = (3, 0, 6)\lambda_c$ is assigned so that after time-modulation they present a focal spot around that point. The resulting field distributions in the plane $y = 0$ are plotted in Fig. 12. In this case, the overall field-level maximum has been found to be located in a small spot located just in front of the array, at the carrier frequency, as denoted by the magenta circle in Fig. 12c.

4 Conclusion

The side-frequency components generated by Time Modulated Arrays have been exploited to generate different simultaneous focal spots in the radiative near field region of a transmitting array antennawhile keeping its original focal spot at the carrier frequency. By doing so, different frequencies may be assigned to different users, hence leading to a potential multi-user system allowing to feed different devices through Wireless Power Transfer, with a particular implementation suitable for much simpler adaptive features, as adaptive

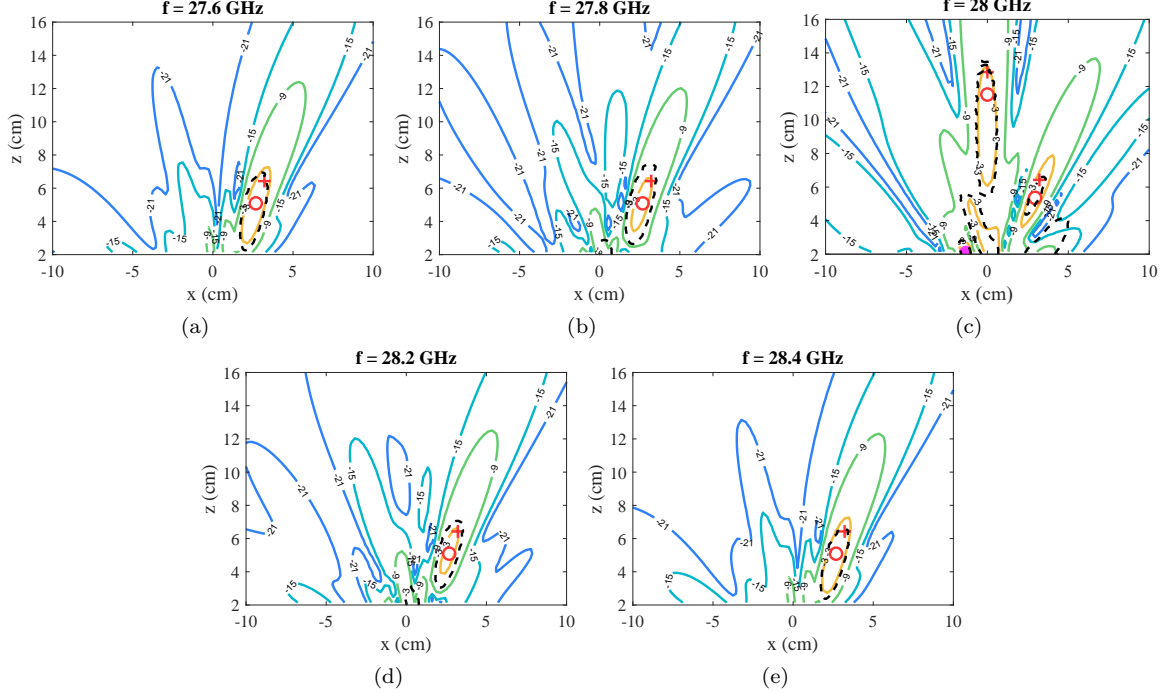


Figure 12: Simulation #4. Normalized Near Field distribution at $y = 0$ with a focal point at $(x, y, z) = (3, 0, 6)\lambda_c$ at all the considered frequencies, and two spots in the carrier at $(x, y, z) = (3, 0, 6)\lambda_c$ and $(0, 0, 12)\lambda_c$. The field level at each frequency is normalized with respect to the overall maximum level. The symbols $+$ and \circ represent the assigned focal point and the synthesized field maximum point, respectively. The contour of the -3dB spot is denoted by the brown line. The -3dB spot obtained through full-wave simulations is denoted by the black dashed line.

radio-frequency hardware may be substituted with digital controllers.

The dependence of the resulting effective weights with the parameters of the control signals is ruled by a very specific formulation. Since the requirements are more demanding with respect to those for conventional multi-focus near-field focused phased arrays, as simultaneous multi-focusing must be achieved at a set of different frequencies of the transmitted signal spectrum, a degradation of the array focusing capabilities was expected. However, some numerical results showed that satisfactory results can still be achieved. Obviously, increasing the number of elements of the array also increases the available degrees of freedom, hence compensating in some sense for the more demanding requirements. An optimized synthesis method for the pulse parameters would probably lead to a better exploitation of the focusing capabilities of Time Modulated Arrays so that the performance gap between them and conventional arrays may get smaller. Finally, work is in progress to extend the narrowband approximation presented here to a wideband formulation, and to investigate the combination of the proposed multi-focus-TMA concept with the novel backscatter modulation technique based on time-varying intelligent reflecting surfaces, which has been recently proposed by Yurduseven et al. in [23].

References

- [1] D. Masotti, M. Shanawani, and A. Costanzo, *Smart Beamforming Techniques for “On Demand” WPT*. John Wiley and Sons, Ltd, 2020, ch. 3, pp. 57–84.
- [2] G. Monti, A. Costanzo, F. Mastri, M. Mongiardo, and L. Tarricone, “Rigorous design of matched wireless power transfer links based on inductive coupling,” *Radio Science*, vol. 51, no. 6, pp. 858–867, June 2016.

Freq	Focal point	DoF	WoF	$ \tilde{E} _{dB}$	$ \tilde{E}_r _{dB}$
27.6 GHz	$(-0, 0, 8)\lambda_c$	5.6	1.0	-1.9	-0.8
27.8 GHz	$(-4, 0, 8)\lambda_c$	5.3	0.8	-2.8	-0.9
	$(5, 0, 5)\lambda_c$	4.9	1.3	-1.6	-1.5
28.2 GHz	$(0, 0, 8)\lambda_c$	7.5	1.1	-1.2	-0.7
28.4 GHz	$(2, 0, 7)\lambda_c$	3.3	0.6	-2.9	-0.7

Table 6: Simulation #3. Depth and width of focus, in cm, for the case with five users at four frequencies. The normalized field amplitude at the focus with respect to the overall maximum (located in the carrier), $|\tilde{E}|$, and relative to the peak value in the focal spot at the same frequency, $|\tilde{E}_r|$, are also shown (in dB).

- [3] A. Costanzo and D. Masotti, “Smart solutions in smart spaces: Getting the most from far-field wireless power transfer,” *IEEE Microwave Magazine*, vol. 17, no. 5, pp. 30–45, May 2016.
- [4] R. Hansen, “Focal region characteristics of focused array antennas,” *IEEE Transactions on Antennas and Propagation*, vol. 33, no. 12, pp. 1328–1337, December 1985.
- [5] P. Nepa, A. Buffi, A. Michel, and G. Manara, “Technologies for near-field focused microwave antennas,” *International Journal of Antennas and Propagation*, vol. 2017, p. 17 pages, 2017.
- [6] M. R. Pino, R. G. Ayestarán, P. Nepa, and G. Manara, “An overview on synthesis techniques for near-field focused antennas,” in *Recent Wireless Power Transfer Technologies*, P. Pinho, Ed. Rijeka: IntechOpen, 2020, ch. 1. [Online]. Available: <https://doi.org/10.5772/intechopen.89600>
- [7] P. Nepa and A. Buffi, “Near-field-focused microwave antennas: Near-field shaping and implementation.” *IEEE Antennas and Propagation Magazine*, vol. 59, no. 3, pp. 42–53, June 2017.
- [8] J. Alvarez, R. G. Ayestaran, and F. Las-Heras, “Design of antenna arrays for near-field focusing requirements using optimisation,” *Electronics Letters*, vol. 48, no. 21, pp. 1323–1325, October 2012.
- [9] J. Alvarez, R. G. Ayestaran, G. Leon, L. F. Herran, A. Arboleya, J. A. Lopez-Fernandez, and F. Las-Heras, “Near field multifocusing on antenna arrays via non-convex optimisation,” *IET Microwaves, Antennas Propagation*, vol. 8, no. 10, pp. 754–764, July 2014.
- [10] R. González Ayestarán, G. León, M. R. Pino, and P. Nepa, “Wireless power transfer through simultaneous near-field focusing and far-field synthesis,” *IEEE Transactions on Antennas and Propagation*, vol. 67, no. 8, pp. 5623–5633, Aug 2019.
- [11] L. Poli, P. Rocca, L. Manica, and A. Massa, “Time modulated planar arrays - analysis and optimisation of the sideband radiations,” *IET Microwaves, Antennas Propagation*, vol. 4, no. 9, pp. 1165–1171, Sep. 2010.
- [12] —, “Pattern synthesis in time-modulated linear arrays through pulse shifting,” *IET Microwaves, Antennas Propagation*, vol. 4, no. 9, pp. 1157–1164, Sep. 2010.
- [13] L. Poli, P. Rocca, G. Oliveri, and A. Massa, “Harmonic beamforming in time-modulated linear arrays,” *IEEE Transactions on Antennas and Propagation*, vol. 59, no. 7, pp. 2538–2545, July 2011.
- [14] R. Maneiro-Catoira, J. Brégains, J. García-Naya, and L. Castedo, “Time modulated arrays: From their origin to their utilization in wireless communication systems,” *Sensors*, vol. 17, no. 3, p. 590, Mar 2017. [Online]. Available: <http://dx.doi.org/10.3390/s17030590>
- [15] D. Masotti, P. Francia, A. Costanzo, and V. Rizzoli, “Rigorous electromagnetic/circuit-level analysis of time-modulated linear arrays,” *IEEE Transactions on Antennas and Propagation*, vol. 61, no. 11, pp. 5465–5474, 2013.

- [16] D. Masotti, A. Costanzo, M. Del Prete, and V. Rizzoli, “Time-modulation of linear arrays for real-time reconfigurable wireless power transmission,” *IEEE Transactions on Microwave Theory and Techniques*, vol. 64, no. 2, pp. 331–342, 2016.
- [17] E. J. Rothwell and M. J. Cloud, *Electromagnetics*, third edition. ed. Boca Raton: CRC Press, Taylor and Francis Group, 2018.
- [18] J. Guo, L. Poli, M. A. Hannan, P. Rocca, S. Yang, and A. Massa, “Time-modulated arrays for physical layer secure communications: Optimization-based synthesis and experimental assessment,” *IEEE Transactions on Antennas and Propagation*, vol. 66, no. 12, pp. 6939–6949, 2018.
- [19] R. J. Mailloux, *Phased Array Antenna Handbook*, 3rd ed. USA: Artech House, Inc., 2017.
- [20] H. Chou, M. R. Pino, P. Nepa, and C. Liu, “Near-field focused subarrays in a multi-panel configuration,” *IEEE Access*, vol. 7, pp. 143 097–143 108, 2019.
- [21] R. González Ayestarán, J. Álvarez, and F. Las-Heras, “Design of non-uniform antenna arrays for improved near-field multifocusing,” *Sensors*, vol. 19, no. 3, p. 645, Feb 2019.
- [22] A. Buffi, P. Nepa, and G. Manara, “Design criteria for near-field-focused planar arrays,” *IEEE Antennas and Propagation Magazine*, vol. 54, no. 1, pp. 40–50, Feb 2012.
- [23] O. Yurduseven, S. D. Assimonis, and M. Matthaiou, “Intelligent reflecting surfaces with spatial modulation: An electromagnetic perspective,” *IEEE Open Journal of the Communications Society*, vol. 1, pp. 1256–1266, 2020.